Comparison between GPM and disdrometers rainfall and drop size distribution products

Author: Sabina Angeloni[a*], Supervisor: Vincenzo Capozzi[b]

[a]National Research Council of Italy, Institute of Atmospheric Sciences and Climate (CNR-ISAC), 00133 Rome, Italy
[b]Department of Science and Technology, University of Naples "Parthenope", 80143 Centro Direzionale di Napoli, Italy
[*]Correspondence: sabina.angeloni@artov.isac.cnr.it

Abstract

Precipitation monitoring is crucial for understanding Earth's climate system and its impacts on various sectors such as hydrology, water management, and agriculture. Satellite-based measurements, particularly through missions like the Global Precipitation Measurement (GPM), have significantly enhanced our ability to observe precipitation patterns globally. The GPM mission, a collaborative effort between NASA and JAXA, employs a dual-frequency precipitation radar onboard the Core Observatory to provide comprehensive observations of rain and snow. This article focuses on validating GPM Dual-frequency Precipitation Radar (DPR) Level 2 Version 7 products over Italy using three ground-based laser disdrometers, located in Turin, Rome, and Montevergine Observatory. Statistical indices are used to assess the agreement between satellite observations and disdrometer data.

Keywords

Global Precipitation Measurement mission; ground validation; disdrometer; Italy

1 Introduction

Precipitation is a fundamental component of Earth's climate system and the accuracy of its measurements is crucial for scientific research and practical applications. Being a critical part of the water cycle, its measurements are essential in hydrological modeling, water resource management and agriculture.

In this context, satellite-based measurements play an important role in improving our understanding of precipitation patterns and their impact. They allow to cover remote and oceanic areas that are challenging to access through ground-based devices, which provide direct measurements of precipitation at specific locations and are limited to land areas. Satellite data are useful in the monitoring of extreme precipitation events, enabling the improvement of forecasting models which enhance the ability to mitigate the impact of these hazards. Satellite observations contribute to climate research and modeling, which needs of accurate input data to simulate future trends.

The Global Precipitation Measurement (GPM) mission [1] of the National Aeronautics and Space Administration (NASA) and Japan Aerospace eXploration Agency (JAXA) involves an international network of satellites to provide next-generation global observation of rain and snow. It centers around the Core Observatory (CO) satellite equipped with an advanced radar system, which serves as a reference standard to unify precipitation measurements from a constellation of research and operational satellites.
It was launched on February 27th, 2014, building upon the success of the Tropical Rainfall Measuring Mission (TRMM) of the same agencies, with respect to which has expanded capabilities

that improve our ability to monitor precipitation across the globe. In particular, while TRMM was operating between 35°S and 35°N using radar at Ku-band [2], the GPM Core Observatory extends coverage to higher latitudes, ranging from 65°S to 65°N, providing a near-global view of precipitation. Moreover, GPM enables the measurements of light rain, solid precipitation and the microphysical properties of falling particles, as well as heavy to moderate rain. It also adopted a dual-frequency precipitation radar (DPR) using two frequencies at the Ku-bands (13.6 GHz) and Ka-bands (35.5 GHz).

Validating satellite-based precipitation measurements is crucial to ensure their accuracy and reliability. Satellite data are compared with ground-based observations, typically provided by rain gauges and radar, and the agreement between them is estimated by using statistical metrics which assess how well satellite products capture the spatial and temporal variability of precipitation. In this context, the GPM mission developed the Ground Validation (GV) program which aims to validate and improve precipitation retrieval algorithms [3]. These purposes are accomplished by means of physical and statistical validations, and products assessment for hydro-meteorological application, in order to optimize their use in hydrological studies.
Since the availability of GPM data, there are many studies concerning the validation of DPR surface rainfall products. An accurate report of the main works can be found in [4]. Even if rain gauges and radars are the most common instruments used as ground-based references, disdrometers are able to provide the microphysical structure of hydrometeors in terms of drop size distribution (DSD) and can be used to validate DPR retrievals at the surface level.

This work aims to use laser disdrometers to validate GPM DPR Level 2 Version 7 products over Italy to compare the GPM-DPR rainfall and DSD parameters with the corresponding ones measured at ground during satellite overpasses between May 22, 2018, and November 6, 2023. The disdrometers are located in different sites, namely Turin in Northern Italy, Rome in Central Italy, and Montevergine Observatory in Southern Italy.

This article is organized as follows. Section 2 provides information regarding GPM DPR and disdrometers. Section 3 explains the processing methods used in the study and the comparison approach. Section 4 presents the main results obtained by comparing the GPM measurements with the ones measured at ground by disdrometers during precipitation events. Finally, Section 5 points out the main findings which are summarized and commented.

2 Intruments and data

2.1 GPM DPR

Onboard the GPM Core Observatory, a key instrument is the Dual-frequency Precipitation Radar (DPR), consisting of the Ku-band Precipitation Radar (KuPR), which operates at 13.6 GHz, and the Ka-band precipitation radar (KaPR) at 35.5 GHz. The KuPR is an upgraded version of the successful unit deployed on the Tropical Rainfall Measuring Mission (TRMM). Aligned on the GPM spacecraft bus, the KuPR and KaPR ensure consistent 5-km footprint locations on Earth. The DPR provides accurate rainfall measurements, surpassing its TRMM predecessor, particularly in detecting light rainfall and snowfall in mid-latitude regions. Rain/snow determination exploits the differential attenuation between Ku-band and Ka-band frequencies. The variable pulse repetition frequency (VPRF) technique enhances sensitivity to 0.2 mm/h, enabling effective measurements. The KuPR and KaPR instruments facilitate rain sensing over land and ocean, day and night. GPM DPR offers products tailored to various scan modes and algorithms, providing flexibility in data processing. The single-frequency (SF) option utilizes data from one of the two radars, while the dual-frequency (DF) one employs data from both radar frequencies.

The 07A version is the first standard product to incorporate the scan pattern modification for the KaPR implemented on May 21, 2018. This change in the scan pattern enables the application of a more precise method for estimating precipitation using the dual-frequency radar across the entire observation swath. Conversely, this shift prompted substantial modifications in DPR file

specifications, affecting common file structures both before and after the scan change, along with algorithm advancements.

In the V07, a new data format is employed for information collected both preceding and subsequent to the alteration in the KaPR scan pattern in May 2018. This updated format incorporates the designation "FS", denoting the full swath dual-frequency product with a range resolution of 125 m. The scan pattern encompasses 49 footprints of approximately 5 km in diameter, resulting in a swath coverage of 245 km. It's important to note that the DPR/FS features single-frequency data from KuPR in the outer swath before the scan pattern adjustment, while it incorporates dual-frequency data in the outer swath post the scan pattern modification.

Moreover, a new 3-D precipitation judgement method is implemented to improve the detectability of precipitation signals. This approach utilizes signals not only in the vertical direction but also in the cross-track and along-track directions, aiming to improve the detection of weak, horizontally distributed precipitation that often occurs at high-latitudes. Additional details about the updates in the new version V07 can be found in [5], which is the reference source of information about the precipitation Level 2 (L2) products (version V07A) used in this study.

All precipitation products are derived through a common modular process, yet notable distinctions in modules differentiate DF from SF products. The main functions of each module (identified by italic capital letters) are described in the following.

The Preparation (PRE) module prepares raw Level 1 input products and external information for utilization by the remaining modules. It calculates reflectivity factors, minimizes clutter influence, identifies the clutter-free bin closest to the terrain, and classifies pixels with precipitation for further processing. Moreover, it supplies measurements of the normalized surface cross-section (NRCS) used in attenuation correction and surface type classification. The Vertical Profile (VER) module computes path-integrated attenuation caused by non-precipitation particles using ancillary environmental data from the Japan Meteorological Agency Global Analysis (JMA-GANAL), such as pressure, temperature, water vapor, and cloud liquid water. The Classification (CSF) module categorizes precipitation types and offers insights into bright-band (for SF products) or melting layer (for DF products) through distinct algorithms, presenting at least three primary classes: stratiform, convective, and "other." The Drop Size Distributions (DSD) module is pivotal, defining physical variables related to precipitation particles, including density, dielectric constants, falling velocity, and the relations employed by the solver module. Based on diverse CSF outputs, a profile is segmented through nodes implying the utilization of various particle models. Typically, particles are modeled as a mixture of air, water, and ice expressed with distinct volume ratios. The drop size distribution is presumed to follow a normalized gamma model

$$N(D) = N_{\mathrm{w}} D^{\mu} \exp\left[-\frac{(4+\mu)D}{D_{\mathrm{m}}}\right] \tag{1}$$

with the fixed shape parameter μ set to 3, necessitating solely N_{w} and D_{m} to characterize the DSD. This simplification is deemed suitable for dual-frequency radar retrievals relying on Ku- and Ka-frequency band measurements [6]. It is important to note that the gamma DSD assumption, even with three parameters, is widespread but not universally appropriate [7]. The Surface Reference Technique (SRT) module computes path-integrated attenuation (PIA) due to propagation through precipitation using radar returns from the surface. Finally, the Solver (SLV) module derives DSD parameters and precipitation rates at each range bin.

This study uses the DF-based 2ADPR-FS, the SF-based 2AKa-FS and 2AKu-FS Version 7 Level 2 DPR products. GPM data from May 22, 2018, to November 7, 2023, are analyzed, since two orbit maneuvers were executed around the latter date, raising the satellite altitude from 400 km to 435 km.

Among the various output variables present in the 2ADPR and 2AKu/2AKa products, specific parameters are used for comparative analysis. These include precipRateNearSurface (RNS), representing the precipitation rate ($\mathrm{mm{\cdot}h^{-1}}$) estimated at the clutter-free bin nearest to the surface (binClutterFreeBottom, CFB); zFactorCorrectedNearSurface (ZNS), indicating the reflectivity factor with attenuation correction (in dBZ) at the CFB; and paramDSD, comprising the normalized gamma drop size distribution (DSD) parameters N_{w} (in $\mathrm{mm^{-1}{\cdot}m^{-3}}$) and D_{m}

(in mm), evaluated at the CFB (for more details on these products, refer to [5]). The mean height of the CFB above the considered disdrometers varies between 1.32 km and 2.10 km, depending on the orography around the disdrometer and the GPM product under consideration. GPM algorithms generate estimates at a bin corresponding to the surface level (binRealSurface) through extrapolation. To assess the efficacy of this extrapolation, we compared rainfall rate, D_{m}, and N_{w} obtained at the CFB with those extrapolated at the binRealSurface level for the locations of the considered disdrometers. The comparison reveals minimal differences between GPM estimates at the CFB and those extrapolated at ground level, with a Normalized Mean Absolute Error (NMAE) less than 1% for DSD parameters and less than 8% for the rainfall rate. Consequently, in this article, we will solely consider the GPM products at the CFB. Furthermore, to isolate rainy overpasses, the height of the CFB is compared with that of the bottom of the bright band (binBBBottom, BBB) and with the height of the melting layer bin (binDFRmMLBottom, MLB). In cases where BBB or MLB data is unavailable, the forecasted height of the 0°C isotherm is considered.

2.2 Disdrometers

Nowadays, the use of disdrometers in precipitation measurement is increasing thanks to their capability to provide the microphysical structure of hydrometeors in terms of drop size distribution and other properties, rather than in terms of precipitation accumulation as provided by raingauges. This study considers three laser disdrometers manufactured by Thies Clima GmbH, Germany, which belong to the Italian Group of Disdrometry (in Italian named Gruppo Italiano Disdrometria, hereafter GID) network, a community-driven initiative to federate disdrometers belonging to different actors that at the moment cover most of the Italian territory [8]. The first one was installed during 2006 in Turin (hereinafter TC-TO) and is the older version of the Thies Clima disdrometer. The second one was installed during 2012 on the roof of the building of the Institute of Atmospheric Sciences and Climate (ISAC) of the National Research Council (CNR) of Italy in Rome (hereinafter TC-RM). The third one was installed in December 2018 on the roof of the Montevergine's monastery and is part of the Montevergine meteorological observatory (hereinafter TC-MV). The owner of the TC-TO and TC-RM is the Regional Agency for the Protection of the Environment of Piemonte (ARPA Piemonte), while University of Naples Parthenope owns the TC-MV. Further information regarding the disdrometers used in this study are reported in Table 1.

Table 1: Information regarding the disdrometers used in this study.

Label	**Site**	**Latitude**	**Longitude**	**Height ASL**
TC-TO	Turin	45.0294	7.6549	250 m
TC-RM	Rome	41.8425	12.6464	102 m
TC-MV	Montevergine Obs.	40.9365	14.7291	1280 m

All the devices store data over one minute, and the datasets undergo pre-processing using a standardized procedure, mainly based on a filter criterion which allows to remove spurious drops caused by wind effects, splashing, or mismatching, together with non-liquid hydrometeors. This filter eliminates drops with a fall velocity outside the 50% range of the theoretical diameter-fall velocity relation, based on [9], taking into account air density according to [10]. The formula for this relation is

$$v\left(D,h\right)=\left(9.65-10.3e^{-0.6D}\right)\left(\frac{\rho(0)}{\rho(h)}\right)^{0.37+0.025D} \tag{2}$$

where $\rho(0)$ and $\rho\left(h\right)$ in kg·m^{-3} are the air density at sea level and at height above sea level h (in m), respectively, that can be assumed according to the International Standard Atmosphere Model [11]. Moreover, only 1-minute samples containing at least 11 drops are considered for

computation. Then the drop size distribution can be expressed (in $\mathrm{mm}^{-1}\cdot\ \mathrm{m}^{-3}$) as

$$N(D_i) = \frac{1}{A\,\Delta t\,\Delta D_i}\sum_{j=1}^{C_\mathrm{v}}\frac{n_{i,j}}{v_j}, \tag{3}$$

where Δt is the sampling time (60 s), A is the measuring area (m^2), v is the fall velocity (expressed in $\mathrm{m{\cdot}s}^{-1}$) from the theoretical diameter-fall velocity relation (2), ΔD is the width of the size bin, $n_{i,j}$ is the number of drops measured in the i-th diameter class and j-th fall velocity class, and C_v is the total number of fall velocity bins. The width of each diameter class is provided by the Thies Clima.
To focus solely on liquid precipitation samples, an air temperature criterion is added to the fall velocity one, which consists in eliminating the measured rainfall records with air temperature below 4°C. Finally, for each DSD, the radar reflectivity factor at Ka- and Ku-band (Z_Ka and Z_Ku, respectively, in $\mathrm{mm}^6{\cdot}\mathrm{m}^{-3}$), the rain rate R (in $\mathrm{mm{\cdot}h}^{-1}$), and the DSD parameters D_m (in mm) and N_w (in $\mathrm{mm}^{-1}{\cdot}\mathrm{m}^{-3}$) can be computed as

$$Z_\mathrm{Ka,Ku} = \frac{\lambda^4\,10^{18}}{\pi^5\,|K_w|^2}\sum_{D_\mathrm{min}}^{D_\mathrm{max}}\sigma_\mathrm{Ka,Ku}(D)\,N(D)\,dD \tag{4}$$

$$R = 6\,\pi\,10^{-4}\sum_{D_\mathrm{min}}^{D_\mathrm{max}} v(D)\,N(D)\,D^3\,dD \tag{5}$$

$$D_\mathrm{m} = \frac{\sum_{D_\mathrm{min}}^{D_\mathrm{max}} N(D)\,D^4\,dD}{\sum_{D_\mathrm{min}}^{D_\mathrm{max}} N(D)\,D^3\,dD} \tag{6}$$

$$N_\mathrm{w} = \frac{256}{\pi\,\rho_\mathrm{w}}\frac{10^3\,LWC}{D_\mathrm{m}^4} \tag{7}$$

$$LWC = \frac{\pi 10^{-3}}{6}\rho_\mathrm{w}\sum_{D_\mathrm{min}}^{D_\mathrm{max}} N(D)\,D^3\,dD \tag{8}$$

where LWC is the liquid water content, λ is the wavelength (in m), K_w is the complex dielectric constant of water, ρ_w is the density of water ($1\ \mathrm{g{\cdot}cm}^{-3}$), and $\sigma_\mathrm{Ku,Ka}$(D) are the backscattering radar cross-section (in m^2) for Ku- and Ka-band of a drop of equivalent diameter D. The scattering properties of hydrometeors depend on various factors, such as composition, shape, orientation, size of the scatters, and the radar wavelength. For this study, the T-matrix method [12, 13] is used to compute the backscattering cross-section of oblate hydrometeors.

3 Comparison approach

There are various strategies that allow comparing ground point measurements with satellite area measurements. In this study, both the point-wise and mean methods, previously employed in [4], will be used. The point-wise method involves comparing the measurement from the disdrometer with the satellite measurement corresponding to the ground pixel containing the coordinates of the considered disdrometer. As discussed above, the DPR estimates at the CFB will be considered rather than those corresponding to the binRealSurface. In this type of comparison, the point-wise disdrometric measurement is considered for the entire reference surface area, which can be source of errors in the analysis. The second method aims to overcome this issue by considering the average of DPR pixels whose centers are at most 5 km away from the disdrometer.

Only the overpasses from May 22, 2018, to November 7, 2023, containing at least one pixel with RNS exceeding 0.1 $\mathrm{mm{\cdot}h}^{-1}$ among the selected ones were retained. The comparison of GPM measurements, representing a ground footprint of approximately 5 km × 5 km, with

point-wise disdrometer data is facilitated by taking the temporal average of the disdrometer time series over a 10-minute window (with a minimum requirement of 3 consecutive disdrometer samples for inclusion in the average). Additionally, the minimum rain rate threshold applied to the disdrometer has been set at 0.1 mm·h^{-1}.

Table 2: Information regarding the number of GPM overpasses with rain and of matched disdrometer and DPR data for point and mean comparison.

GPM product	**# overpasses with rain**	**# matched data (point)**	**# matched data (mean)**
DPR	92	40	47
Ku	91	40	46
Ka	72	36	40

Examining all the usable samples, Table 2 displays the count of matched disdrometer records and GPM overpasses: for each DPR product, the first column shown the number of overpasses with rain (i.e. with at least one pixel, within 5 km from disdrometer, with RNS>0.1 mm·h^{-1}); the number of matched disdrometer and DPR data for point and mean comparison are reported in the second and third columns, respectively. It is worth noting that the overpasses associated with the Ka product are fewer compared to the other products, due to the fact that the Ka band has low sensitivity to very small rain rate values. The evaluation encompasses both rainfall (Z, R) and DSD parameters (D_m and N_w). Finally, the agreement between satellite and disdrometer measurements is assessed calculating statistical parameters. The Normalized Mean Absolute Error (NMAE, in %) provides a measure of the accuracy, being calculated as the ratio of the Mean Absolute Error (MAE) to the standard deviation of the reference variable. This index provides a standardized measure of the mean absolute error, making it easier to compare models or predictions on different scales of magnitude. The Normalized Bias (NB) provides information on the quality of the difference of the two datasets (satellite and ground-based): negative NB values indicate an underestimation of the GPM product with respect to the disdrometer measurement. The correlation coefficient measures the degree to which the two sets of data are linearly related. It assumes values in the range from -1 to $+1$, where ± 1 indicates the strongest possible agreement and 0 the strongest possible disagreement.

4 Results

In this section, the results of the comparison analysis between GPM-DPR and disdrometer precipitation measurements are presented, according to the methods and criteria previously defined.

Figure 1 shows the scatterplots between rainfall rates R, radar reflectivity factors Z (Ku- and Ka-bands) and DSD parameters (D_m and $10 \log_{10} N_\mathrm{w}$) obtained from GPM and disdrometer data. The merit parameters obtained from the comparison between satellite and ground-based data using point and mean methods as defined in Section 3 are reported in Table 3 and 4, respectively. For the reflectivity factor Z, the merit parameters related to the DPR product have been calculated considering both the Ka- and Ku-bands together. A graphical representation of the merit parameters is given in Figure 2.

The rainfall rate R is characterized by maximum NMAE values, especially for the Ka-FS product (92.3%). Furthermore, the DPR product shows the minimum NMAE value both in point and mean comparison (57.5% and 59.3%, respectively). The correlation of the rainfall rate is 0.70 for the DPR product with point comparison and is lower for the other products. The point comparison determines a widely positive bias for all products, which tends to decrease in the mean comparison, becoming even negative in the case of the Ka product and equal to -2.7%.

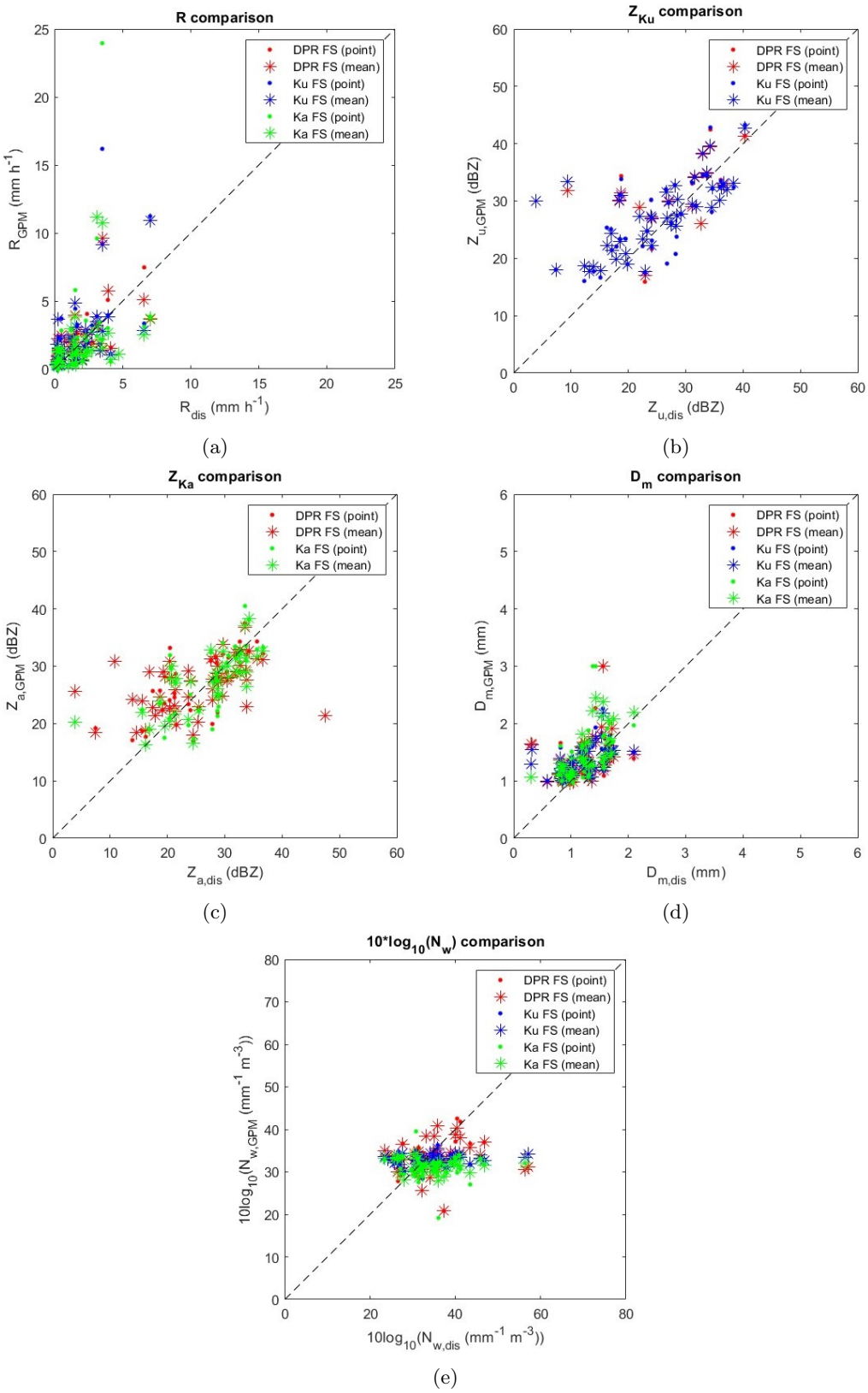

Figure 1: Scatterplot between **(a)** rainfall rate, **(b)-(c)** reflectivity factor, **(d)** D_{m}, and **(e)** $10\log_{10} N_{\mathrm{w}}$ obtained from disdrometers (x-axis) and GPM products (y-axis) listed in the legend, by using the point (point markers) and mean (star markers) methods.

Table 3: Merit parameters of the comparison between GPM and disdrometer data related to the point comparison mode. NMAE and NB are in %, while MAE is in the same unit of the variable ($\mathrm{mm \cdot h^{-1}}$ for R, dBZ for Z, mm for D_m and $\mathrm{mm^{-1} \cdot m^{-3}}$ for N_w). Correlation is dimensionless.

		NMAE	**MAE**	**NB**	**corr**
R	DPR FS	57.5	0.96	15.6	0.70
	Ku FS	80.1	1.34	33.7	0.58
	Ka FS	92.3	1.77	27.4	0.35
Z	DPR FS	15.8	4.10	4.2	0.72
	Ku FS	17.6	4.51	5.9	0.74
	Ka FS	13.0	3.53	0.3	0.71
D_m	DPR FS	24.4	0.30	11.6	0.49
	Ku FS	21.3	0.26	10.4	0.55
	Ka FS	24.4	0.31	17.5	0.52
$10 \log_{10} N_\mathrm{w}$	DPR FS	13.0	4.43	-3.4	0.32
	Ku FS	13.7	4.65	-3.4	0.07
	Ka FS	17.1	5.86	-9.3	-0.14

Table 4: Merit parameters of the comparison between GPM and disdrometer data related to the mean comparison mode. The units of the parameters are the same as in the caption of Table 3.

		NMAE	**MAE**	**NB**	**corr**
R	DPR FS	59.3	0.94	14.7	0.64
	Ku FS	65.2	1.03	23.0	0.66
	Ka FS	73.4	1.39	-2.7	0.39
Z	DPR FS	18.4	4.67	7.0	0.61
	Ku FS	19.7	4.88	10.8	0.67
	Ka FS	13.2	3.51	1.7	0.72
D_m	DPR FS	26.3	0.31	12.6	0.35
	Ku FS	24.3	0.29	12.5	0.48
	Ka FS	23.5	0.29	17.5	0.65
$10 \log_{10} N_\mathrm{w}$	DPR FS	15.2	5.29	-4.2	0.08
	Ku FS	14.3	5.02	-6.3	0.25
	Ka FS	16.5	5.72	-9.4	-0.02

The reflectivity factor Z generally exhibits the best performance in terms of merit parameters. The NMAE values are among the lowest, ranging between 13.0% and 19.7%. A slight positive bias is observed for all products and comparison modes. The correlation is the highest among all parameters, with the maximum value equal to 0.74 for the Ku product in the point comparison.

The DSD parameters generally exhibit lower correlation values compared to those related to rainfall parameters, with minima reached by the variable $10 \log_{10} N_\mathrm{w}$. In the latter case, the Ka product shows a negative correlation, equal to -0.14 in the point mode and -0.02 in the mean mode. Figures 1d and 1e show a positive bias for the variable D_m and a negative bias for $10 \log_{10} N_\mathrm{w}$, in both cases more pronounced for the Ka product (up to 17.5% and -9.4%, respectively). The NMAE values range between 21.3% and 26.3% for the D_m variable and between 13% and 17.1% for $10 \log_{10} N_\mathrm{w}$. Finally, D_m has the minimum MAE values for all

GPM products and all comparison methods, while for the $10\log_{10} N_{\mathrm{w}}$ the highest MAE values are obtained, especially for the Ka product (equal to 5.86 and 5.72, using the point and mean mode, respectively).

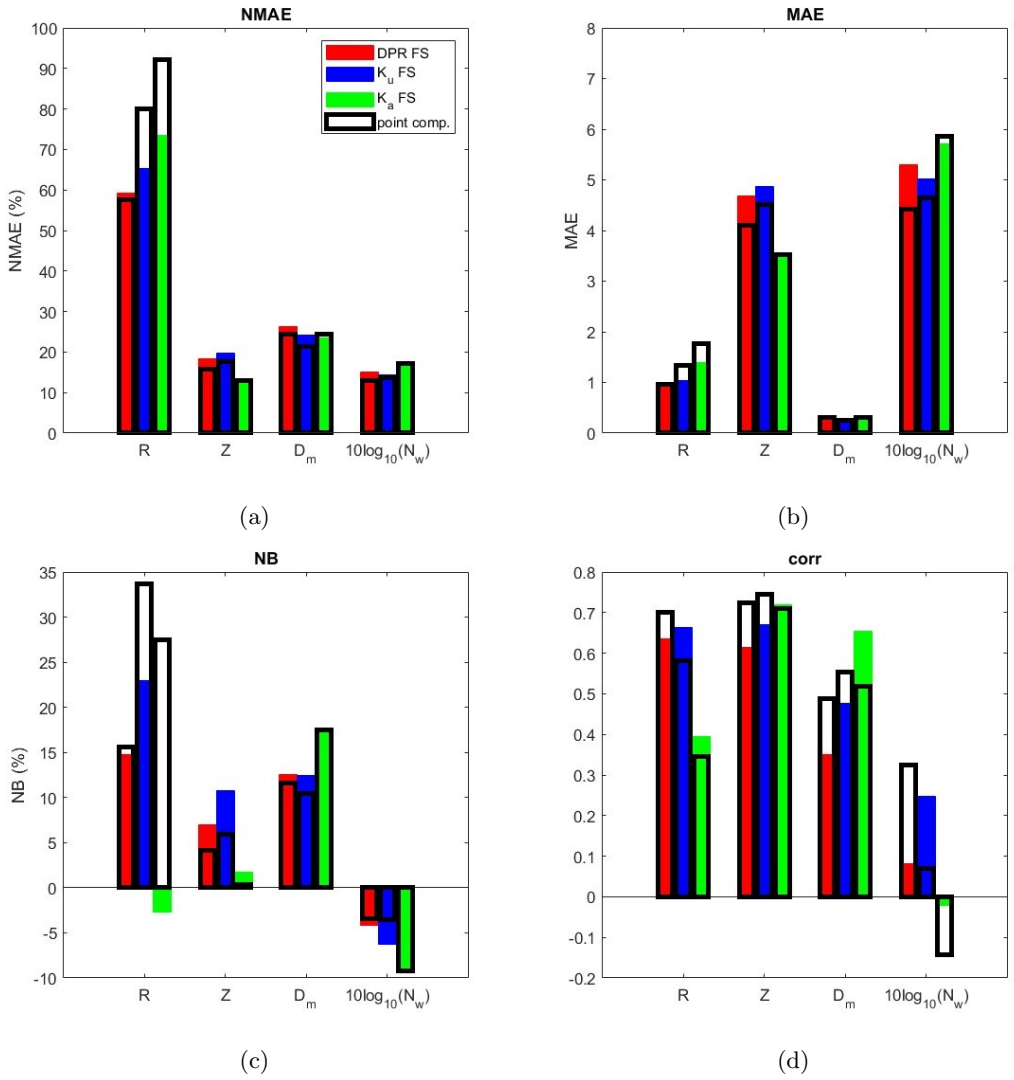

Figure 2: Graphical representation of **(a)** NMAE, **(b)** MAE, **(c)** NB and **(d)** corr for each parameter R, Z, D_{m} and $10\log_{10} N_{\mathrm{w}}$ (x-axis) obtained by disdrometers and GPM products. The colored bar consider the mean comparison, while the grey edge bars are for the point comparison.

A greater dispersion of the data for the variable R and Z is referred to the overpasses on the disdrometer at the Montevergine Observatory. Figure 3 shows scatterplots of rainfall parameters when considering only the disdrometer data from Montevergine and when these are excluded from the ground-based dataset (thus considering only the data from the disdrometers in Rome and Turin). As can be observed from the comparison between the merit parameters depicted in the Figure 3 and those in the Tables 3 and 4, the Montevergine dataset yields worse scores. Removing the data from this site leads to a significant improvement in all merit parameters. The reasons why the Montevergine dataset shows greater differences with GPM measurements could be related to the spatial variability of precipitation around the site and the impact of wind on disdrometers [14], considering the different morphological nature of the terrain compared to

the other sites considered in this study.

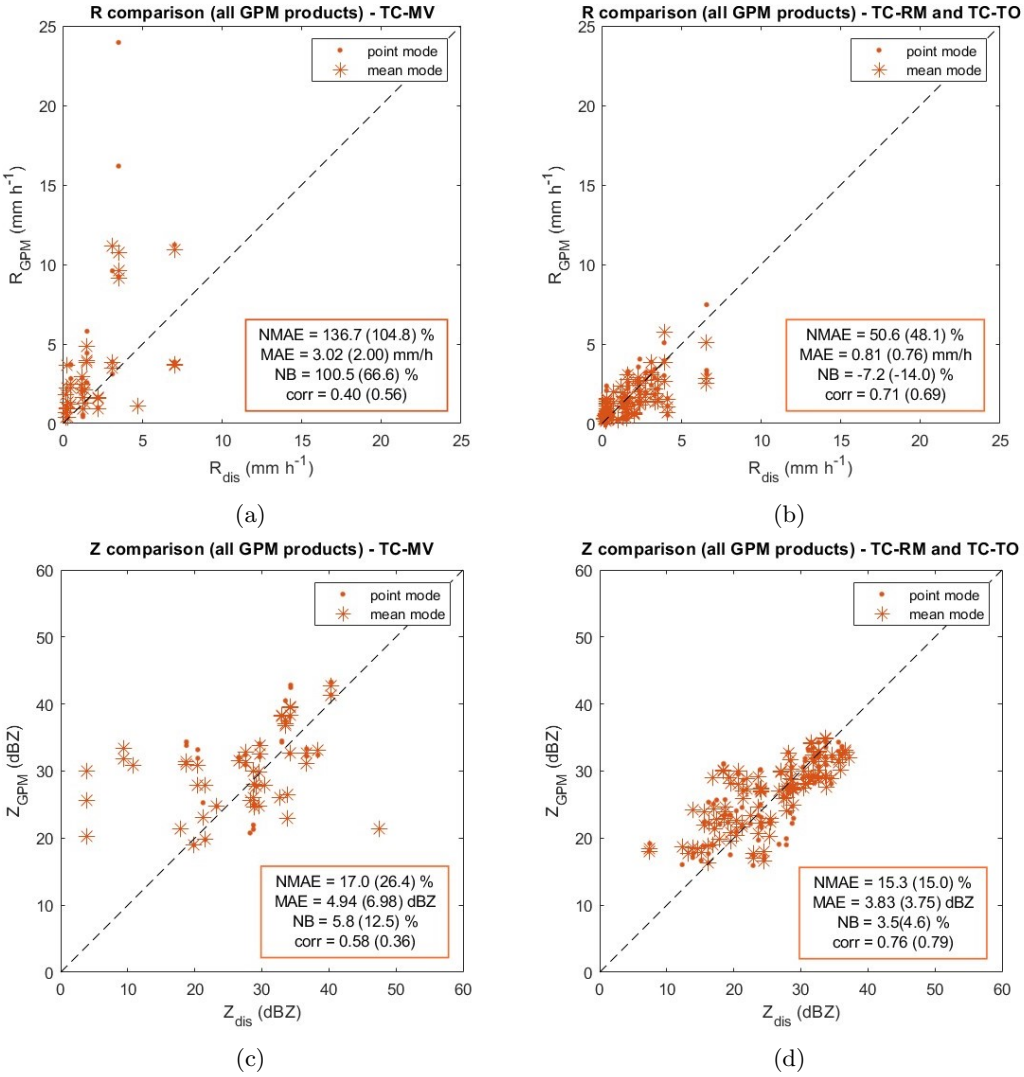

Figure 3: Scatterplot between rainfall rate (top graphics) and reflectivity factor (bottom graphics) obtained from disdrometers (x-axis) and GPM products (y-axis) by using the point (point markers) and mean (star markers) methods. **a** and **c** refers to TC-MV disdrometer, while **b** and **d** to both TC-RM and TC-TO. At the bottom right of each graph, the merit parameters are reported for point (and mean) mode.

5 Conclusions

The analysis of satellite-based precipitation measurements, particularly those from the Global Precipitation Measurement (GPM) mission, underscores their critical role in enhancing our understanding of precipitation patterns and their impacts. Through advanced radar systems and international collaboration, GPM provides comprehensive coverage, extending from remote and oceanic areas to higher latitudes, thus offering a near-global view of precipitation phenomena. This expanded coverage, coupled with improved capabilities for detecting various precipitation types and microphysical properties, yields a significant advancement over preceding missions like the Tropical Rainfall Measuring Mission (TRMM).

Validation of satellite-derived precipitation data remains paramount to ensure their accuracy and reliability. The Ground Validation (GV) program associated with GPM aims to refine precipitation retrieval algorithms through rigorous comparisons with ground-based observations, including rain gauges, radar, and laser disdrometers. These validation efforts are crucial for optimizing the use of satellite data in hydrological modeling and other applications.

The study presented herein focuses on validating GPM Dual-frequency Precipitation Radar (DPR) Level 2 Version 7 products over Italy using laser disdrometers located across different regions. Comparative analyses reveal notable performance metrics, with radar reflectivity factors demonstrating particularly strong correlations and relatively low error rates across various products and comparison methods. However, there are disparities in the performance of rainfall and microphysical parameters, which are more pronounced in cases related to GPM passes over the Montevergine Observatory, probably related to the spatial variability of precipitation around this site and the impact of wind on disdrometers. Based on these preliminary results, a partial improvement in scores compared to the Version 6 is observed. However, further studies are necessary, including a greater number of disdrometers to be used as ground reference instruments and other comparison methods, in order to outline a more robust framework that allows for separately analyzing the convective and stratiform cases, providing additional evaluation elements regarding the performance of GPM measurements.

Acknowledgments

I would like to express my sincere gratitude to Luca Baldini and Elisa Adirosi for providing the satellite data and materials used for the comparison of GPM DPR Level 2 Version 6 products.

References

[1] Hou, A. Y.; et al. (2014): The Global Precipitation Measurement Mission. *Bull. Amer. Meteor. Soc., 95,* 701–722, https://doi.org/10.1175/BAMS-D-13-00164.1.

[2] Kummerow, C.; Barnes, W.; Kozu, T.; Shiue, J.; Simpson, J. (1998): The Tropical Rainfall Measuring Mission (TRMM) Sensor Package. *J. Atmos. Oceanic Technol., 15,* 809–817, https://doi.org/10.1175/1520-0426(1998)015¡0809:TTRMMT¿2.0.CO;2.

[3] Schwaller, M. R.; Morris, K. R. (2011): A Ground Validation Network for the Global Precipitation Measurement Mission. *J. Atmos. Oceanic Technol., 28,* 301–319, https://doi.org/10.1175/2010JTECHA1403.1.

[4] Adirosi, E.; et al. (2021): Validation of GPM Rainfall and Drop Size Distribution Products through Disdrometers in Italy. *Remote Sens., 13,* 2081, https://doi.org/10.3390/rs13112081.

[5] Iguchi, T.; Seto, S.; Meneghini, R.; Yoshida, N.; Awaka, J.; Le, M.; Chandrasekar, V.; Brodzik, S.; Tanelli, S.; Kanemaru, K.; Masaki, T.; Kubota, T.; Takahashi, N. (2023): GPM/DPR Level-2 Algorithm Theoretical Basis Document.

[6] Liao, L.; Meneghini, R.; Tokay, A. (2014): Uncertainties of GPM DPR rain estimates caused by DSD parameterizations. *J. Appl. Meteorol. Climatol., 53,* 2524–2537, https://doi.org/10.1175/JAMC-D-14-0003.1.

[7] Adirosi, E.; Volpi, E.; Lombardo, F.; Baldini, L. (2016): Raindrop size distribution: Fitting performance of common theoretical models. *Adv. Water Resour., 96,* 290–305, https://doi.org/10.1016/j.advwatres.2016.07.010.

[8] Adirosi, E.; Porcù, F.; Montopoli, M.; Baldini, L.; Bracci, A.; Capozzi, V.; Annella, C.; Budillon, G.; Bucchignani, E.; Zollo, A. L.; et al. (2023): Database of the Italian Disdrometer Network. *Earth System Science Data*, *15*, 2417–2429, https://doi.org/10.5194/essd-15-2417-2023.

[9] Gunn, R.; Kinzer, G. D. (1949): The terminal velocity of fall for water droplets in stagnant air. *Journal of Meteorology*, *6*, 243–248, https://doi.org/10.1175/1520-0469(1949)006¡0243:ttvoff¿2.0.co;2.

[10] Foote, G. B.; Du Toit, P. S. (1969): Terminal Velocity of Raindrops Aloft. *Journal of Applied Meteorology*, *8*, 249–253, https://doi.org/10.1175/1520-0450(1969)008¡0249:tvora¿2.0.co;2.

[11] Porcù, F.; D'Adderio, L. P.; Prodi, F.; Caracciolo, C. (2014): Rain Drop Size Distribution over the Tibetan Plateau. *Atmospheric Research*, *150*, 21–30. https://doi.org/10.1016/j.atmosres.2014.07.005.

[12] Barber, P.W.; Yen, C. (1975): Scattering of electromagnetic waves by arbitrarily shaped dielectric bodies. *Appl. Opt., 14,* 2864–2872, https://doi.org/10.1364/AO.14.002864.

[13] Mishchenko, M.I.; Travis, L.D.; Mackowski, D.W. (1996): T-matrix computations of light scattering by nonspherical particles: A review. *J. Quant. Spectrosc. Radiat. Transf., 55,* 535–575, https://doi.org/10.1016/0022-4073(96)00002-7.

[14] Capozzi V.; Annella C.; Montopoli M.; Adirosi E.; Fusco G.; Budillon G. (2021): Influence of Wind-Induced Effects on Laser Disdrometer Measurements: Analysis and Compensation Strategies. *Remote Sensing.* 13(15):3028, https://doi.org/10.3390/rs13153028.